Mutations in the Nucleotide Binding Domain of the α Subunits of the F_1-ATPase from Thermophilic *Bacillus* PS3 That Affect Cross-Talk between Nucleotide Binding Sites†

Neil B. Grodsky, Chao Dou, and William S. Allison*

Department of Chemistry and Biochemistry, School of Medicine, University of California at San Diego, La Jolla, California 92093-0601

Received September 22, 1997; Revised Manuscript Received November 17, 1997

ABSTRACT: Inactivation of MF_1 (bovine mitochondrial F_1-ATPase) with 5′-*p*-fluorosulfonylbenzoyl-ethenoadenosine is caused by labeling αY244 [Verburg, J. G., and Allison, W. S. (1990) *J. Biol. Chem. 265*, 8065−8074]. In the crystal structure [Abrahams, J. P., Leslie, A. G. W., Lutter, R., and Walker, J. E. (1994) *Nature 370*, 621−628], αY244 is hydrogen bonded to αR304 which is also hydrogen bonded to αY300. The catalytic properties of mutant $\alpha_3\beta_3\gamma$ subcomplexes of the TF_1-ATPase from the thermophilic *Bacillus* PS3 containing the αF244C, αR304C, and αY300C substitutions have been examined. Each has unique features for hydrolyzing ATP and forming inhibitory ADP−fluoroaluminate complexes in catalytic sites. Unlike wild-type, the $(\alpha R304C)_3\beta_3\gamma$ and $(\alpha Y300C)_3\beta_3\gamma$ subcomplexes entrap inhibitory MgADP in a catalytic site during turnover which fails to dissociate when ATP binds to noncatalytic sites. Although the hydrolytic properties of the $(\alpha F244C)_3\beta_3\gamma$ subcomplex and wild-type are similar, the mutant forms ADP−fluoroaluminate complexes 7 times faster than wild-type when Al^{3+} and F^- are added to it in the presence of excess ADP and Mg^{2+}. It also resists inhibition by high Mg^{2+} concentrations in the assay medium. At least one noncatalytic site of the $(\alpha F244C)_3\beta_3\gamma$ subcomplex has increased affinity for ADP, indicating that the enhanced rate of formation of the ADP−fluoroaluminate complex reflects augmented cooperativity between noncatalytic and catalytic sites. The rate of formation of the ADP−fluoroaluminate complex in $(\alpha Y300C)_3\beta_3\gamma$ increases only 40% when MgADP in bound to two catalytic sites rather than one, compared to a 9-fold increase exhibited by wild type. When Al^{3+} and F^- are added to the $(\alpha Y300C)_3\beta_3\gamma$ subcomplex after incubation with excess ADP and Mg^{2+}, ADP−fluoroaluminate complexes are formed in three catalytic sites rather than two observed with the other subcomplexes. Reconciliation of the catalytic properties of the mutant subcomplexes in terms of the crystal structure suggests that αF244, αR304, and αY300 of TF_1 are part of a pathway that propagates conformational signals from one catalytic site to another.

The F_oF_1-ATP synthases of energy transducing membranes couple proton electrochemical gradients to the condensation of ADP and P_i. The F_1 moiety is a peripheral membrane protein complex. When removed from the membrane, F_1 is an ATPase (*1*). Five gene products comprise the F_1-ATPases which are present in a stoichiometry of $\alpha_3\beta_3\gamma\delta\epsilon$. They contain six nucleotide binding sites. Three are catalytic, and the other three, for which a defined functional role remains to be elucidated, are known as noncatalytic sites (*2, 3*). The catalytic sites are present mostly on β subunits, but also contain residues contributed from adjacent α subunits. On the other hand, noncatalytic sites are mostly in α subunits, but contain residues contributed from adjacent β subunits (*4*). In the crystal structure, the catalytic sites are heterogeneously liganded as follows: subunit β_E has no bound nucleotide in the catalytic site, β_{DP} has MgADP bound to the catalytic site, and β_{TP} has MgAMP−PNP bound to the catalytic site. The α subunits, each of which is liganded with MgAMP−PNP, are denoted as follows: α_E contributes to the catalytic site of β_E, α_{DP} contributes to the catalytic site of β_{DP}, and α_{TP} contributes to the catalytic site of β_{TP}. The α and β subunits are folded nearly identically into three domains: top (amino-terminal), middle (nucleotide binding), and bottom (carboxyl-terminal).

The $\alpha_3\beta_3\gamma$ subcomplex of TF_1[1] has catalytic characteristics similar to those of the complete enzyme (*5*−*8*). Therefore, comparing the catalytic properties of the wild-type and mutant $\alpha_3\beta_3\gamma$ subcomplexes of TF_1 is appropriate for examining structure−function relationships in F_1-ATPases. Moreover, a plasmid containing the genes encoding the α, β, and γ subunits of TF_1 can be overexpressed in an unc^- strain of *Escherichia coli* to produce the assembled $\alpha_3\beta_3\gamma$ complex in high yield (*9*).

† This work was supported by United States Public Health Service Grant GM-16974 (to W.S.A.).

* To whom correspondence should be addressed. Telephone: (619) 534-3057. Fax: (619) 822-0079. E-mail: wallison@ucsd.edu.

[1] Abbreviations: TF_1 and MF_1, F_1-ATPases from thermophilic *Bacillus* PS3 and bovine heart mitochondria, respectively; FSBεA, 5′-*p*-fluorosulfonylbenzoylethenoadenosine; FSBA, 5′-*p*-fluorosulfonylbenzoyladenosine; TPCK, *N*-tosyl-L-phenylalanine chloromethyl ketone; CDTA, *trans*-1,2-diaminocyclohexane-*N*,*N*,*N*′,*N*′-tetraacteic acid; HPLC, high-performance liquid chromatography; LDAO, lauryl dimethylamine oxide; TF_oF_1, F_oF_1-ATPase from thermophilic *Bacillus* PS3.

S0006-2960(97)02349-0 CCC: $15.00
Published on Web 01/08/1998

Steady-state kinetic analysis of ATP hydrolysis by F_1-ATPases is complicated by turnover-dependent entrapment of inhibitory MgADP in a catalytic site. When noncatalytic sites are not saturated with ATP, three kinetic phases are observed when MF_1, TF_1, and the $\alpha_3\beta_3\gamma$ subcomplex of TF_1 hydrolyze low concentrations of ATP (*7*, *10*, *11*). An initial burst rapidly decelerates to a slow intermediate rate that gradually accelerates to a final steady-state rate which approaches the initial rate. Transition from the burst to the slow intermediate phase is caused by turnover-dependent entrapment of MgADP in a single catalytic site (*12*, *13*). Slow binding of ATP to noncatalytic sites promotes dissociation of MgADP from the affected catalytic site. This is responsible for transition from the intermediate phase to the final rate (*7*, *10*, *11*).

An earlier study (*14*) showed that derivatization of Tyr244 in a single copy of the α subunit accompanies inactivation of MF_1 by FSBϵA. From this observation, it was concluded that αTyr244 is part of the noncatalytic nucleotide binding site. However, when the X-ray structure of MF_1 was subsequently deduced (*4*), it was clear that αTyr244 is not part of the noncatalytic nucleotide binding site. Instead, αTyr244 is located in a cluster of conserved aromatic side chains in the nucleotide binding domain but is distant from the nucleotide binding site. In MF_1 these residues are αTyr244, αTyr248, αTyr278, and αTyr300. In the crystal structure, the phenolic oxygen of αTyr244 is hydrogen bonded to the guanidinium of αArg304 which in turn is hydrogen bonded to the phenolic oxygen of αTyr300. In TF_1, a phenylalanine is present in the position occupied by αTyr244 in MF_1. The residue numbers of MF_1 are used here to designate residues in the α and β subunits of TF_1 and *E. coli* F_1. Also an indication that this site plays a functional role in catalysis, Omote et al. (*15*) reported that the second site mutation, αR304C, partly rescues activity in the βS181F mutant of *E. coli* F_1. In the crystal structure of MF_1, βSer181 is 29.7 Å from αR304C, clearly ruling out a direct interaction between these residues. Hartog et al. (*16*) recently reported that both αTyr244 and αTyr300 are derivatized along with βTyr368 when MF_1 is inactivated with FSBA in the presence of 10% glycerol which further implies that these residues have a functional role in catalysis. The combined observations provoked further examination of this region of the α subunit by site-directed mutagenesis. Following the observation of Omote et al. (*15*) that the αR304C mutant of *E. coli* F_1 has slightly less than half the membrane-bound ATPase activity of wild-type, single mutants have been generated in the $\alpha_3\beta_3\gamma$ subcomplex of TF_1 in which αPhe244, αArg304, and αTyr300 were substituted with cysteine. The catalytic properties of the mutant enzymes have been compared with those of wild-type under a variety of conditions.

EXPERIMENTAL PROCEDURES

Materials. TPCK-treated trypsin, enzymes used in assays, chemicals, biochemicals, and buffer components were purchased from Sigma, unless noted otherwise. [^{3}H]ADP was obtained from DuPont New England Nuclear. 2-N_3-[^{3}H]-ADP was synthesized as previously described (*17*). LDAO was supplied by Calbiochem. Sodium fluoride was obtained from Aldrich, and solutions of it were prepared and stored in plastic containers. Aluminum chloride was purchased from Fisher Scientific. Sephadex G-50 was supplied by Pharmacia. The oligonucleotides used for mutagenesis were purchased from Gibco BRL. Restriction enzymes were purchased from Promega or New England Biolabs.

The wild-type $\alpha_3\beta_3\gamma$ subcomplex and the $(\alpha F244C)_3\beta_3\gamma$, $(\alpha Y300C)_3\beta_3\gamma$, and $(\alpha R304C)_3\beta_3\gamma$ subcomplexes were purified according to Matsui and Yoshida (*9*) after expression in an unc$^-$ strain of *E. coli* from plasmids encoding the β and γ subunits of TF_1, and either the wild-type or mutant α subunits. The complexes were stored as precipitates in 70% saturated ammonium sulfate at 4 °C. Before use in the studies described, samples of the suspensions were pelleted by centrifugation. The pellets were dissolved in 50 mM Tris-HCl (pH 8.0) containing 1 mM CDTA. After being incubated for 30 min to allow chelation of Mg^{2+}, the protein solutions were passed through two consecutive centrifuge columns of Sephadex G-50 which were equilibrated with 50 mM Tris-HCl (pH 8.0) containing 0.1 mM EDTA (*18*). After treatment with CDTA, the subcomplexes were essentially free of endogenous nucleotides as assessed by HPLC.

Methods. Site-directed mutagenesis was performed as described by Kunkel et al. (*19*). The oligonucleotides 5′-AC-ACC-GGC-ATA-TGG-CGC-CAA-GCA-CAA-AAG-CGG-3′, which contained a new site for *Nde*I; 5′-TGC-GCG-CTC-GAG-CAG-GCA-GGA-GTG-CAA-G-3′, which contained a new site for *Xho*I; and 5′-GGA-GTG-CAA-GCA-GAA-GAT-ATC-CCC-CG-3′, which contained a new site for *Eco*RV were used to introduce the αF244C, αR304C, and αY300C substitutions, respectively. The new restriction sites allowed facile screening of the mutants. Restriction mapping showed that the constructed plasmids contained the desired mutations. This was confirmed by DNA sequencing (*20*).

Protein concentrations were determined by the method of Bradford (*21*). ATPase activity was determined spectrophotometrically by an ATP regeneration system (*17*). The rates of conversion of the reversibly inhibited subcomplexes containing MgADP in catalytic sites to the irreversibly inhibited subcomplexes with ADP−fluoroaluminate complexes bound to catalytic sites were determined as previously described (*22*).

RESULTS

Comparison of the Hydrolytic Properties of the $\alpha_3\beta_3\gamma$, $(\alpha F244C)_3\beta_3\gamma$, $(\alpha R304C)_3\beta_3\gamma$, and $(\alpha Y300C)_3\beta_3\gamma$ Subcomplexes. Figure 1 compares hydrolysis of 50 μM ATP by the wild-type and mutant subcomplexes in the presence of an ATP regenerating system before (traces A, C, E, and G) and after (traces B, D, F, and H) incubating each with a slight excess of ADP in the presence of Mg^{2+} in order to load a single catalytic site with MgADP (*7*, *8*). Trace A shows the three kinetic phases exhibited during hydrolysis of 50 μM ATP by the wild-type subcomplex. The final rate of ATP hydrolysis in trace A is 5.8 μmol of ATP mg^{-1} min^{-1}. Trace C illustrates that three kinetic phases are also exhibited during hydrolysis of 50 μM ATP by the $(\alpha F244C)_3\beta_3\gamma$ subcomplex. The final steady-state rate is 5.1 μmol of ATP mg^{-1} min^{-1}. However, in the case of the $(\alpha F244C)_3\beta_3\gamma$ subcomplex, the intermediate phase is more extended than observed with the wild-type subcomplex. In contrast, trace

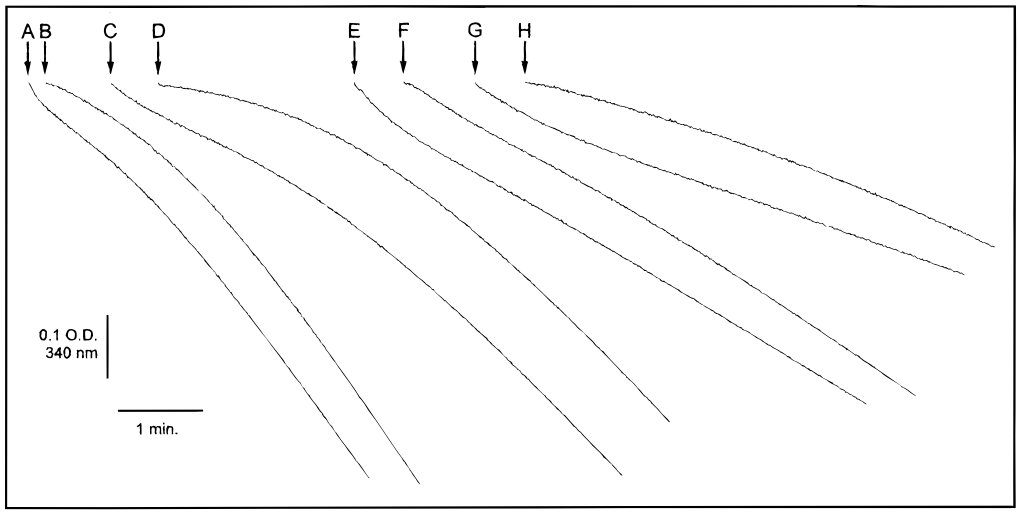

FIGURE 1: Comparison of hydrolysis of 50 μM ATP by the $\alpha_3\beta_3\gamma$, $(\alpha F244C)_3\beta_3\gamma$, $(\alpha R304C)_3\beta_3\gamma$, and $(\alpha Y300C)_3\beta_3\gamma$ subcomplexes. Solutions, 1 mg/mL each, of the wild-type and mutant subcomplexes were prepared in 50 mM Tris-HCl (pH 8.0) containing 0.1 mM EDTA with 3 μM ADP (B, D, F, and H) or without ADP (A, C, E, and G). Then, 8 μL samples of the wild-type (A and B), $(\alpha F244C)_3\beta_3\gamma$ (C and D), $(\alpha R304C)_3\beta_3\gamma$ (E and F), or $(\alpha Y300C)_3\beta_3\gamma$ (G and H) subcomplexes were withdrawn and injected into 1 mL of assay medium containing 50 μM ATP and 1.05 mM Mg^{2+} using the coupled system described in Experimental Procedures.

Table 1: Effects of LDAO and Increasing Mg^{2+} Concentration on the Rate of Hydrolysis of 2 mM ATP by the Wild-Type and Mutant Subcomplexes[a]

subcomplex	specific activity[b]	LDAO	$[Mg^{2+}]$ 2 mM	4 mM	5 mM	10 mM
wild-type	20[c]	74	22.9	16.9	14.5	11.8
$(\alpha F244C)_3\beta_3\gamma$	15	36	15.1	14.4	14.3	13.4
$(\alpha R304C)_3\beta_3\gamma$	6.2	43	8.6	4.3	3.6	2.4
$(\alpha Y300C)_3\beta_3\gamma$	5.5	12	6.4	3.4	2.7	1.8

[a] Enzyme stock solutions, 1 mg/mL, were prepared in 50 mM Tris-HCl (pH 8.0) containing 0.1 mM EDTA. For the LDAO experiment, samples, 1 μL each of the wild-type or $(\alpha F244C)_3\beta_3\gamma$ subcomplexes or 5 μL each of the $(\alpha R304C)_3\beta_3\gamma$ or $(\alpha Y300C)_3\beta_3\gamma$ mutant subcomplexes, were assayed in medium containing 2 mM ATP and 3 mM Mg^{2+} and 0.06% LDAO. For the Mg^{2+} experiment, 5 μL samples of the wild-type or mutants subcomplexes were assayed in medium containing 2 mM ATP and the concentrations of Mg^{2+} specified. [b] This column also represents "3 mM Mg^{2+}" for the effect of increasing Mg^{2+} concentration. [c] Specific activities are shown with units micromoles of ATP hydrolyzed per minute per milligram.

E illustrates that only two kinetic phases are observed when the $(\alpha R304C)_3\beta_3\gamma$ subcomplex hydrolyzes 50 μM ATP. An initial burst decelerates to a slow, constant rate of 2.4 μmol of ATP mg^{-1} min^{-1}, which is equivalent to the intermediate phase observed for the wild-type subcomplex. Trace G shows that two kinetic phases are also observed when the $(\alpha Y300C)_3\beta_3\gamma$ subcomplex hydrolyzes 50 μM ATP. The final steady-state rate is 2.3 μmol of ATP mg^{-1} min^{-1}. Traces B, D, F, and H illustrate hydrolysis of 50 mM ATP by the wild-type $\alpha_3\beta_3\gamma$ and $(\alpha F244C)_3\beta_3\gamma$, $(\alpha R304C)_3\beta_3\gamma$, and $(\alpha Y300C)_3\beta_3\gamma$ subcomplexes, respectively, after loading a single catalytic site of each with MgADP. In all cases, an extended lag precedes attainment of the final steady-state rate. However, the rate of ATP hydrolysis catalyzed by the wild-type subcomplex accelerates much more rapidly than that observed with the mutant subcomplexes.

Table 1 shows that the nonionic detergent LDAO stimulates the ATPase activity of the wild-type subcomplex by nearly 4-fold (*6*, *7*), whereas the $(\alpha R304C)_3\beta_3\gamma$ subcomplex is stimulated nearly 7-fold by the presence of 0.06% LDAO. The stimulatory effect of LDAO on the ATPase activities of the $(\alpha F244C)_3\beta_3\gamma$ and $(\alpha Y300C)_3\beta_3\gamma$ subcomplexes is 2.4- and 2.2-fold, respectively. Plotting ATPase activity vs increasing LDAO concentrations (data not shown) shows that the stimulation of the subcomplexes by LDAO plateaus between 0.05 and 0.1% LDAO.

Treatment of the $(\alpha Y300C)_3\beta_3\gamma$ subcomplex with either 10 mM iodoacetamide or 10 mM *N*-ethylmaleimide for 30 min prior to assay increased V_{max} from 5.5 to 11.5 and 16 μmol of ATP min^{-1} mg^{-1}, respectively. V_{max} of the $(\alpha R304C)_3\beta_3\gamma$ subcomplex was increased from 6.2 to 11 μmol of ATP min^{-1} mg^{-1} upon treatment with 10 mM *N*-ethylmaleimide; however, 10 mM iodoacetamide did not affect the V_{max} of the $(\alpha R304C)_3\beta_3\gamma$ subcomplex. Neither reagent affected the V_{max} of the $(\alpha F244C)_3\beta_3\gamma$ subcomplex. Presumably, the stimulations observed are caused by derivatization of the introduced cysteines. It is worth noting here that the αF244C/αR304C mutant plasmid was prepared but failed to express an assembled $(\alpha F244C)_3/(\alpha R304C)_3\beta_3\gamma$ subcomplex. After expression in *E. coli*, only the isolated β subunit was obtained from the bacterial lysates.

Comparison of Increasing Concentrations of Mg^{2+} in the Assay Medium on Hydrolysis of 2 mM ATP by the Wild-Type and Mutant Subcomplexes. It has been shown that turnover-dependent inhibition of CF_1, MF_1, and the $\alpha_3\beta_3\gamma$ subcomplex of TF_1 caused by entrapment of inhibitory MgADP in a catalytic site during ATP hydrolysis increases as the concentration of free Mg^{2+} in the assay medium is increased (*8*, *23*, *24*). Since the results in Figure 1 suggest that the $(\alpha R304C)_3\beta_3\gamma$ and $(\alpha Y300C)_3\beta_3\gamma$ subcomplexes entrap inhibitory MgADP in a catalytic site during turnover to a greater extent than wild-type, the effects of increasing the concentration of free Mg^{2+} in the assay medium on the rate of hydrolysis of 2 mM ATP were examined. Table 1 shows that, as the concentration of Mg^{2+} in the assay medium increases, the rate of hydrolysis of 2 mM ATP by the $(\alpha R304C)_3\beta_3\gamma$ and $(\alpha Y300C)_3\beta_3\gamma$ subcomplexes decreases to a greater extent than that observed for wild-type. In

Table 2: Rates of Formation of ADP−Fluoroaluminate Complexes by the Wild-Type and Mutant Subcomplexes under Various Conditions[a]

subcomplex	ADP added (mol:mol)	k_{inact} (min^{-1}) nothing added	2 mM P_i added	10 mM SO_3^{2-} added
wild-type	1:1	4.2×10^{-3}	$<10^{-4}$	3.3×10^{-3} (0.79)
$(\alpha F244C)_3\beta_3\gamma$	1:1	1.6×10^{-3}	$<10^{-4}$	2.2×10^{-3} (1.4)
$(\alpha R304C)_3\beta_3\gamma$	1:1	6.0×10^{-3}	$<10^{-4}$	5.5×10^{-3} (0.92)
$(\alpha Y300C)_3\beta_3\gamma$	1:1	9.9×10^{-3}	$<10^{-4}$	8.6×10^{-3} (0.88)
wild-type	2:1	3.8×10^{-2} (9.0)[b]	3.2×10^{-3} (0.76)	2.7×10^{-2} (6.4)
$(\alpha F244C)_3\beta_3\gamma$	2:1	1.4×10^{-2} (8.7)	3.5×10^{-3} (2.19)	1.1×10^{-2} (6.9)
$(\alpha R304C)_3\beta_3\gamma$	2:1	3.2×10^{-2} (5.3)	4.7×10^{-3} (0.78)	2.0×10^{-2} (3.3)
$(\alpha Y300C)_3\beta_3\gamma$	2:1	1.4×10^{-2} (1.4)	8.5×10^{-3} (0.86)	9.6×10^{-3} (0.97)
wild-type	200 μM	5.5×10^{-2} (13)	3.6×10^{-1} (86)	5.4×10^{-1} (130)
$(\alpha F244C)_3\beta_3\gamma$	200 μM	1.5×10^{-1} (94)	1.1[c] (690)	1.2[c] (750)
$(\alpha R304C)_3\beta_3\gamma$	200 μM	2.9×10^{-2} (4.8)	2.3×10^{-1} (38)	3.8×10^{-1} (63)
$(\alpha Y300C)_3\beta_3\gamma$	200 μM	1.8×10^{-2} (1.8)	8.6×10^{-2} (8.7)	2.0×10^{-1} (20)

[a] Subcomplexes with MgADP bound to one catalytic site were prepared as follows: 400 μL of 1 mg/mL wild-type, αF244C, αR304C, or αY300C $\alpha_3\beta_3\gamma$ subcomplex in 50 mM Tris-HCl (pH 8.0) containing 0.1 mM EDTA was incubated with 3 μM [^{3}H]ADP and 2 mM $MgCl_2$ for 45 min at room temperature at which time they were passed through 5 mL centrifuge columns of Sephadex G-50 equilibrated with 50 mM Tris-HCl (pH 8.0). The gel-filtered subcomplexes contained 0.89 (wild-type), 0.97 (αF244C), 0.90 (αR304C), and 0.91 (αY300C) mol of [^{3}H]ADP per mole. Each was incubated with 2 mM P_i, 10 mM Na_2SO_3, or no addition in 50 mM Tris-HCl (pH 8.0) or buffer alone before $AlCl_3$ and NaF were added to final concentrations of 200 μM and 5 mM, respectively, to initiate inactivation. Subcomplexes with MgADP bound to two catalytic sites were prepared as described above for the 1:1 ADP−F_1 complexes except that the wild-type and $(\alpha R304C)_3\beta_3\gamma$ subcomplexes were loaded by incubation with 50 μM [^{3}H]ADP, and the $(\alpha F244C)_3\beta_3\gamma$ and $(\alpha Y300C)_3\beta_3\gamma$ subcomplexes were loaded by incubation with 6 μM [^{3}H]ADP. After gel filtration, the 2:1 ADP−F_1 complexes contained 1.9 (wild-type), 1.8 (αF244C), 2.1 (αR304C), and 2.1 (αY300C) mol of [^{3}H]ADP per mole. Inactivation mixtures were prepared as described for the 1:1 ADP−F_1 complexes. For inactivation in the presence of 200 μM ADP, the wild-type and mutant subcomplexes were incubated with 200 μM ADP and 2 mM Mg^{2+} for 45 min before $AlCl_3$ and NaF were added to final concentrations of 200 μM and 5 mM, respectively, to initiate inactivation. Pseudo-first-order rate constants were determined from Guggenheim plots (*39*). [b] Numbers in parentheses represent the rate of inactivation relative to that of the subcomplex with MgADP in a single catalytic site (1:1). [c] Estimated from a single point on Guggenheim plots.

contrast, increasing Mg^{2+} concentration has little effect on the hydrolytic activity of the $(\alpha F244C)_3\beta_3\gamma$ subcomplex.

Comparison of the Rates of Formation of the Inhibitory ADP−Fluoroaluminate Complex by the $\alpha_3\beta_3\gamma$, $(\alpha F244C)_3\beta_3\gamma$, $(\alpha R304C)_3\beta_3\gamma$, and $(\alpha Y300C)_3\beta_3\gamma$ Subcomplexes. The inactive ADP−fluoroaluminate complex is formed slowly when Al^{3+} and F^- are added to the $\alpha_3\beta_3\gamma$ subcomplex of TF_1 or to MF_1 containing MgADP in a single catalytic site (*22*). In contrast, when Al^{3+} and F^- are added to the enzymes containing MgADP bound to two catalytic sites or in the presence of excess ADP and Mg^{2+}, ADP−fluoroaluminate complexes are formed rapidly in two catalytic sites demonstrating catalytic to catalytic site cooperativity. The ADP−fluoroaluminate complexes are formed at different rates with the $\alpha_3\beta_3\gamma$, $(\alpha D269N)_3\beta_3\gamma$, $\alpha_3(\beta T163S)_3\gamma$, and $\alpha_3(\beta Y345W)_3\gamma$ subcomplexes. Therefore, it was pertinent to compare rates of formation of the ADP−fluoroaluminate complexes with the $\alpha_3\beta_3\gamma$, $(\alpha F244C)_3\beta_3\gamma$, $(\alpha R304C)_3\beta_3\gamma$, and $(\alpha Y300C)_3\beta_3\gamma$ subcomplexes.

Table 2 compares the first-order rate constants obtained for inactivation of the wild-type and mutant subcomplexes treated with ADP and Mg^{2+} with or without P_i or SO_3^{2-} before adding Al^{3+} and F^- to them. The wild-type and mutant $(\alpha R304C)_3\beta_3\gamma$ subcomplexes behaved similarly when inactivated by Al^{3+} and F^- in the presence of Mg^{2+} and ADP under the various conditions summarized in Table 2. The rate of inactivation of the $(\alpha R304C)_3\beta_3\gamma$ mutant subcomplex was about 50% of that observed with the wild-type subcomplex under all conditions. Both subcomplexes were inactivated at considerably faster rates when Al^{3+} and F^- were added to enzyme containing MgADP at two catalytic sites rather than one. Furthermore, when Al^{3+} and F^- were added to these subcomplexes after incubation with 200 μM ADP and 2 mM Mg^{2+}, the rate of inactivation was about the same as that observed when the subcomplexes contained MgADP bound to two catalytic sites. The rates of formation of the ADP−fluoroaluminate complexes in $\alpha_3\beta_3\gamma$ and $(\alpha R304C)_3\beta_3\gamma$ containing MgADP in one or two catalytic sites were attenuated in the presence of P_i. On the other hand, the rates of formation of the inactive ADP−fluoroaluminate complexes were accelerated considerably when Al^{3+} and F^- were added to the subcomplexes after prior incubation with 200 μM ADP, 2 mM Mg^{2+}, and 2 mM P_i. Table 2 also shows that the wild-type and $(\alpha R304C)_3\beta_3\gamma$ mutant subcomplexes were inactivated even more rapidly when Al^{3+} and F^- were added after they were incubated with 200 μM ADP, 2 mM Mg^{2+}, and 10 mM SO_3^{2-}.

In contrast, the $(\alpha F244C)_3\beta_3\gamma$ and $(\alpha Y300C)_3\beta_3\gamma$ mutant subcomplexes behaved very differently than the wild-type subcomplex under several of the conditions described in Table 2. Whereas the rate of inactivation of the wild-type accelerated 9-fold when Al^{3+} and F^- were added to it when MgADP was bound to two, opposed to a single catalytic site, the rate of inactivation of the $(\alpha Y300C)_3\beta_3\gamma$ mutant subcomplex was accelerated only 40% when occupancy of catalytic sites with MgADP increased from one to two. Incubation of the wild-type subcomplex with 200 μM ADP, 2 mM Mg^{2+}, and 2 mM P_i increased the rate of inactivation 86-fold over that observed when the subcomplex was loaded with MgADP at a single catalytic site. However, the rate of inactivation of the $(\alpha Y300C)_3\beta_3\gamma$ subcomplex was stimulated only 8.7-fold under the same conditions. The rate of inactivation of the wild-type subcomplex was stimulated 130-fold when Al^{3+} and F^- were added after incubating it with 200 μM ADP, 2 mM Mg^{2+}, and 10 mM SO_3^{2-}, whereas the rate of inactivation of the $(\alpha Y300C)_3\beta_3\gamma$ mutant subcomplex was stimulated only 20-fold under the same conditions.

Table 2 also shows that the rates of inactivation of the wild-type and $(\alpha F244C)_3\beta_3\gamma$ mutant subcomplexes increased

Table 3: Entrapment of [^{3}H]ADP in Fluoroaluminate Complexes during Inactivation of the Wild-Type and Mutant Subcomplexes[a]

	moles of [^{3}H]ADP per mole of subcomplex	
subcomplex	without CDTA	with CDTA
wild-type	1.8	1.9
$(\alpha F244C)_3\beta_3\gamma$	2.7	1.7
$(\alpha R304C)_3\beta_3\gamma$	2.1	2.1
$(\alpha Y300C)_3\beta_3\gamma$	3.0	2.9

[a] The wild-type and mutant $(\alpha F244C)_3\beta_3\gamma$, $(\alpha R304C)_3\beta_3\gamma$, and $(\alpha Y300C)_3\beta_3\gamma$ subcomplexes were incubated with 150 μM [^{3}H]ADP for 30 min in the presence of 2 mM Mg^{2+}, at which time 200 μM $AlCl_3$ and 5 mM NaF were added to initiate the inactivations. When inactivated by 95%, half of each inactivated subcomplex was passed through two successive 1 mL centrifuge columns of Sephadex G-50 equilibrated with 50 mM Tris-HCl (pH 8.0) containing 0.1 mM EDTA to remove unbound [^{3}H]ADP. The other half of each inactivated subcomplex was incubated with 5 mM CDTA for 1 h before application to the centrifuge columns. The protein concentrations and radioactivities of the final effluents were determined as described in Experimental Procedures.

about 9-fold when Al^{3+} and F^- were added to them when MgADP was bound to two catalytic sites rather than one. However, the two subcomplexes behaved very differently when Al^{3+} and F^- were added to them after prior incubation with 200 μM ADP and 2 mM Mg^{2+}. Under these conditions, the rate of inactivation of the $(\alpha F244C)_3\beta_3\gamma$ subcomplex accelerated 94-fold over that observed when MgADP was bound to a single catalytic site. In contrast, the rate of inactivation of the wild-type subcomplex increased only 13-fold under the same conditions. When the mutant $(\alpha F244C)_3\beta_3\gamma$ subcomplex was incubated with 200 μM ADP and 2 mM Mg^{2+} and either 2 mM P_i or 10 mM SO_3^{2-}, prior to the addition of Al^{3+} and F^-, the rate of inactivation accelerated 690- and 750-fold, respectively, over that observed when MgADP was bound to a single catalytic site. Under the same conditions, the presence of 2 mM P_i or 10 mM SO_3^{2-} caused 86- and 130-fold increases, respectively, in the rate of inactivation of the wild-type complex.

Increased Retention of [^{3}H]ADP in a Noncatalytic Site of the $(\alpha F244C)_3\beta_3\gamma$ Subcomplex and in a Catalytic Site of the $(\alpha Y300C)_3\beta_3\gamma$ Subcomplex. Previous studies have shown that, when TF_1 and its $\alpha_3\beta_3\gamma$ subcomplex were incubated with excess ADP and Mg^{2+} and then passed through centrifuge columns of Sephadex G-50, MgADP remained bound to two catalytic sites, whereas noncatalytic sites did not retain ADP (*22*, *25*). It was shown previously that ADP−fluoroaluminate complexes were formed in only two catalytic sites when the wild-type $\alpha_3\beta_3\gamma$ subcomplex was incubated with excess [^{3}H]ADP and Mg^{2+} followed by inactivation initiated on the addition of $AlCl_3$ and NaF (*22*). Table 3 summarizes the results obtained when the mutant $(\alpha F244C)_3\beta_3\gamma$, $(\alpha R304C)_3\beta_3\gamma$, and $(\alpha Y300C)_3\beta_3\gamma$ subcomplexes were treated with 150 μM [^{3}H]ADP and 2 mM Mg^{2+} and then 200 μM Al^{3+} and 5 mM F^- followed by incubation until less than 5% of the ATPase activity remained. Whereas the wild-type and $(\alpha R304C)_3\beta_3\gamma$ subcomplexes retained about 2 mol of [^{3}H]ADP per mole when submitted to this procedure, significantly greater than two sites were occupied with [^{3}H]ADP when the $(\alpha F244C)_3\beta_3\gamma$ and $(\alpha Y300C)_3\beta_3\gamma$ subcomplexes were inactivated under the same conditions. Treatment of the inactive [^{3}H]ADP−fluoroaluminate complexes with CDTA removed about 1 mol of [^{3}H]ADP from the $(\alpha F244C)_3\beta_3\gamma$ subcomplex, but did not remove [^{3}H]ADP from the other subcomplexes.

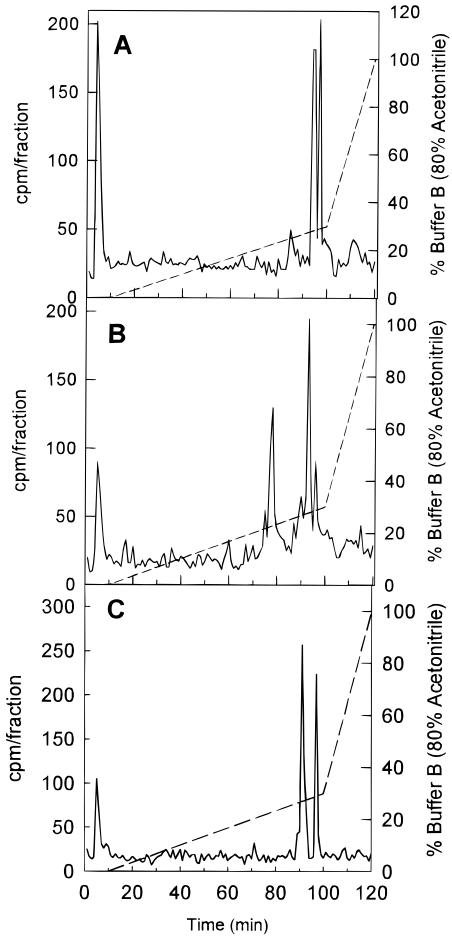

FIGURE 2: Assignment of nucleotide binding sites after loading the $(\alpha F244C)_3\beta_3\gamma$ and $(\alpha Y300C)_3\beta_3\gamma$ subcomplexes with excess 2-N_3-[^{3}H]ADP in the presence of Al^{3+} and F^-. Solutions, 1 mg/mL each, of wild-type (A), $(\alpha F244C)_3\beta_3\gamma$ (B), or $(\alpha Y300C)_3\beta_3\gamma$ (C) in 50 mM Tris-HCl (pH 8.0) containing 0.1 mM EDTA were incubated with 150 μM 2-N_3-[^{3}H]ADP and 2 mM Mg^{2+} in the dark for 1 h before adding 200 μM $AlCl_3$ and 5 mM NaF to initiate inactivation. When inactivated by 95%, the samples were passed through two successive 1 mL centrifuge columns of Sephadex G-50 before irradiating them for 90 min to induce covalent labeling. After irradiation, the enzyme complexes were digested with trypsin and submitted to HPLC on a C_4 reversed-phase column as described previously (*17*).

To determine whether the additional [^{3}H]ADP bound per mole of the inactivated $(\alpha F244C)_3\beta_3\gamma$ and $(\alpha Y300C)_3\beta_3\gamma$ subcomplexes was on a catalytic or a noncatalytic site, fluoroaluminate complexes were prepared containing 2-N_3-[^{3}H]ADP with these subcomplexes as described in the legend of Figure 2. The inactive 2-N_3-[^{3}H]ADP−fluoroaluminate complexes were irradiated and digested with trypsin, and the digests were submitted to reversed-phase HPLC on a C_4 column. Figure 2A shows the pattern of radioactive peptides obtained when the tryptic digest of the derivatized wild-type subcomplex was submitted to HPLC. All peptide-bound radioactivity eluted in two peaks between 90 and 100 min. Since it has been demonstrated that the F_1-ATPases slowly hydrolyze ADP tethered to catalytic sites to tethered AMP in the presence of Mg^{2+} (*26*), these peaks represent the tryptic peptide containing βTyr345 tethered to [^{3}H]AMP and to [^{3}H]-ADP. No radioactivity eluted from the column between 70

and 80 min, the position where the tryptic peptide containing [^{3}H]ADP tethered to βTyr368 elutes using the gradient employed (*17*). Therefore, none of the 2-N_3-[^{3}H]ADP was bound to noncatalytic sites of the wild-type enzyme. In contrast, Figure 2B shows that 70% of the peptide-bound radioactivity eluted between 90 and 100 min and 30% eluted as a single peak between 70 and 80 min when the tryptic digest of the derivatized $(\alpha F244C)_3\beta_3\gamma$ subcomplex was submitted to HPLC under these conditions. This indicates that two catalytic sites and a noncatalytic site of the $(\alpha F244C)_3\beta_3\gamma$ subcomplex were labeled. Figure 2C shows that all of the peptide-bound radioactivity eluted between 90 and 100 min when the tryptic digest of the derivatized $(\alpha Y300C)_3\beta_3\gamma$ subcomplex was submitted to HPLC, indicating that only catalytic sites were photolabeled. The yields of radioactivity in the peptide fractions obtained from the two columns are consistent with the derivatization of two catalytic sites in the wild-type subcomplex, two catalytic sites and a noncatalytic site in the $(\alpha F244C)_3\beta_3\gamma$ subcomplex, and three catalytic sites in the $(\alpha Y300C)_3\beta_3\gamma$ subcomplex. It was shown previously that, after treatment of TF_1 with MgADP bound to three catalytic sites with CDTA and then passage of the enzyme through a centrifuge column, ADP remained bound to only one catalytic site (*25*). Given the fact that [^{3}H]ADP remains bound to three catalytic sites of the $(\alpha Y300C)_3\beta_3\gamma$ subcomplex after incubation with excess ADP, Mg^{2+}, Al^{3+}, and F^- followed by treatment with CDTA, this suggests that the [^{3}H]ADP−fluoroaluminate complex is formed at three catalytic sites of the $(\alpha Y300C)_3\beta_3\gamma$ subcomplex.

DISCUSSION

It is clear from the results presented that the side chains of αY(F)244, αR304, and αY300 are critical for normal function of the $\alpha_3\beta_3\gamma$ subcomplex of TF_1. These results corroborate earlier chemical modification studies showing that the activity of MF_1 is abolished when αY244 is derivatized by FSBεA (*14*) and that modification of both αY244 and αY300 along with βY368 contribute to inactivation of the enzyme by FSBA (*16*). The kinetic characterization of the $(\alpha R304C)_3\beta_3\gamma$ subcomplex presented here extends results reported by Omote et al. (*15*), who showed that the αR304C substitution in *E. coli* F_1 attenuates ATP hydrolysis catalyzed by the membrane-bound enzyme. In the absence of crystal structures of the wild-type and mutant subcomplexes, it is not known whether the altered catalytic properties of the mutant enzymes might be caused by defective folding of the α subunit. However, the stability of the three mutant subcomplexes examined in this study during isolation and storage compared to other mutant subcomplexes suggests that defective folding might not be responsible for the differences in catalytic properties observed. Expression of the plasmid containing the αF244C/αR304C double mutation does not lead to an assembled $\alpha_3\beta_3\gamma$ complex. Two subcomplexes containing substitutions at βM222, which is near αY300 at the α/β interface (*4*), have greatly decreased stability (H.-M. Ren and W. S. Allison, unpublished observations). The βM222C subcomplex dissociates during gel permeation chromatography on Sephacryl S300 HR. The βM222E mutant dissociates during chromatography on Toyopearl Butyl 650-S. In contrast, the three mutant subcomplexes used in this study are isolated in yields comparable to that of wild type and do not dissociate during chromatography on Sephacryl S300 HR and Toyopearl Butyl 650-S, or during storage.

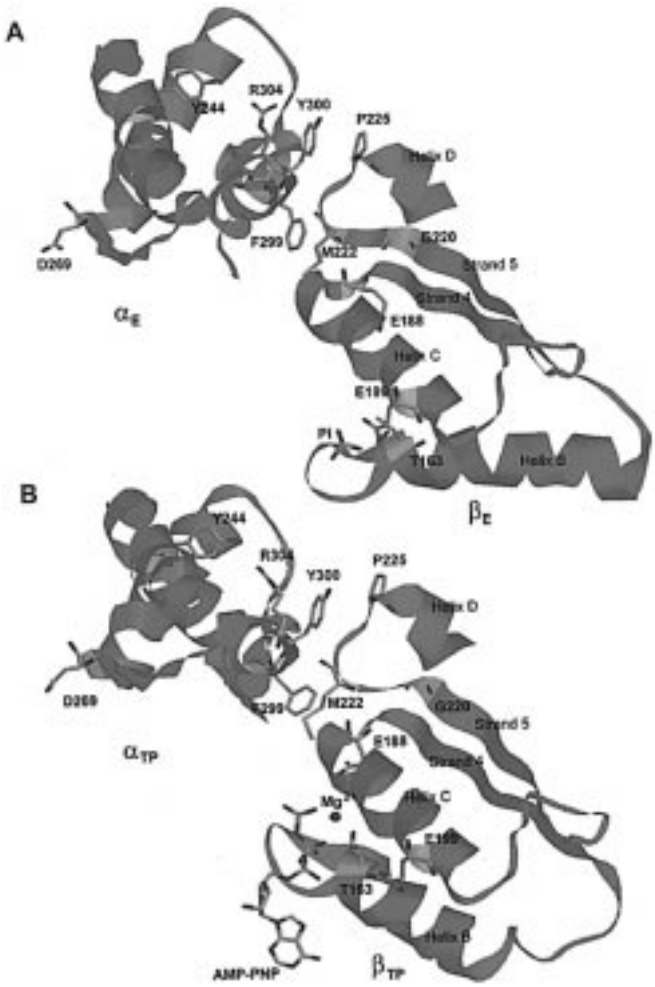

FIGURE 3: Coordinate shifts of αTyr244, αArg304, αTyr300, and other residues at an α/β interface which occur upon liganding of the catalytic site. Panel A represents the α_E/β_E interface, whereas panel B represents the α_{TP}/β_{TP} interface. Residue αD269 is coordinated to the Mg^{2+} in the MgAMP−PNP complex bound to the noncatalytic site. MgAMP−PNP is bound to the catalytic site of β_{TP} (*4*). The residues shown in wireframe are αY244, αD269, αF299, αY300, αR304, βP225, βM222, βG220, βE188, βThr163, and βE199. This figure was generated using the software program Rasmol kindly provided by R. Sayle (Glaxo Wellcome Research and Development, Greenford, U.K.).

Before we comment on functional roles for αY244, αR304, and αY300 in F_1-ATPases, it is instructive to consider the location of these residues in the crystal structure of MF_1 (*4*). The arrangements of αY244, αR304, and αY300 with respect to each other and with respect to the pyrophosphoryl subdomain of the catalytic site are illustrated in Figure 3. In the α_E subunit shown in Figure 3A, the phenolic oxygen of αY244 is within 3.7 Å of the guanidinium of αR304 which, in turn, is 3.9 Å from the phenolic oxygen of αY300. In the α_{TP} subunit shown in Figure 3B and in the α_{DP} subunit not shown, the distances between the phenolic oxygen of αY244 and the guanidinium of αR304 are 3.1 and 3.4 Å, respectively, and the distances between the guanidinium of αR304 and the phenolic oxygen of αY300 are 5.0 and 4.6 Å, respectively. It appears that liganding of catalytic sites with MgADP or MgATP causes

the side chain of αR304 to move from the side chain of αY300 toward the side chain of αY244. Coordinated changes occur at an interface between α and β subunits. Figure 3A shows that the side chain of βPro225 is 3.85 Å from and parallel to the side chain of αTyr300 at the α_E/β_E interface. In contrast, at the α_{TP}/β_{TP} interface illustrated in Figure 3B, αTyr300 and βPro225 are not parallel and are 5.74 Å apart, showing that considerable movement of side chains occurs at this interface as liganding of catalytic sites changes. At the α_{DP}/β_{DP} interface, these residues are 4.13 Å apart and are not parallel. Given that αTyr300 interacts with βPro225 at the α_E/β_E interface, it is possible that the αY300C substitution interrupts transmission of conformational signals between catalytic and noncatalytic sites.

It has been reported that mutations in *E. coli* F_1 at the positions corresponding to βGly220 and βMet222 of MF_1 lead to defective ATPase activity (*27*, *28*). In the crystal structure of MF_1, both of these are located on the same loop as βPro225 illustrated in Figure 3 (*4*). The shifting of the side chain of βGlu188, the catalytic base, with respect to βMet222 on liganding catalytic sites appears to trigger repositioning of side chains in the α subunit. Interestingly, in β_E (Figure 3A), the sulfur of βMet222 is 8.0 Å from the carboxylate of βGlu188, whereas in both β_{TP} (Figure 3B) and β_{DP}, the sulfur atom and carboxylate are only 3.8 Å apart. It should also be noted that the C_ζ of αPhe299 is 12.2 Å from the caboxylate oxygen of βGlu188 in β_E (Figure 3A). However, in β_{TP} (Figure 3B), the C_ζ of αPhe299 is only 5.6 Å from the carboxylate oxygen of βGlu188. The simultaneous shift of βMet222 with respect to βGlu188, of αPhe299 with respect to βGlu188, and of αTyr300 with respect to βPro225 at the α/β interfaces illustrated in panels A and B of Figure 3 might represent part of the pathway for relaying conformational signals from one catalytic site to another during catalysis which travel through the nucleotide binding domains of α subunits.

In β_E (Figure 3A), the hydroxyl oxygen of βThr163, at the end of the Walker A motif (*29*) on helix B, is hydrogen bonded to the carboxylate oxygen of βGlu199 on helix C, the residue that reacts with DCCD in MF_1 (*30*). However in β_{TP} (Figure 3B), helix B shifts relative to helix C on liganding of MgAMP−PNP, which appears to cause βThr163 to move away from βGlu199 and coordinate to the Mg^{2+} bound at the catalytic site. This large shift in the position of the helices relative to each other might be important in initiating conformational signals that are propagated from one catalytic site to another.

It is clear from this study that the αF244C, αR304C, and αY300C substitutions affect cross-talk between noncatalytic and catalytic sites of the $\alpha_3\beta_3\gamma$ subcomplex of TF_1. For instance, the $(\alpha R304C)_3\beta_3\gamma$ and $(\alpha Y300C)_3\beta_3\gamma$ subcomplexes have catalytic characteristics similar to those of the $(\alpha D269N)_3\beta_3\gamma$ subcomplex (*7*). In the crystal structure of MF_1, αD269 is liganded to Mg^{2+} coordinated with AMP−PNP bound to noncatalytic sites (*4*). Although the αD269N substitution does not prevent binding of ATP or ADP to noncatalytic sites of this mutant subcomplex, it retains inhibitory MgADP on a catalytic site when ATP binds to noncatalytic sites (*7*). Similarly, the $(\alpha R304C)_3\beta_3\gamma$ and $(\alpha Y300C)_3\beta_3\gamma$ subcomplexes fail to dissociate inhibitory MgADP from a catalytic site in the presence of saturating ATP, whether it is entrapped during catalysis or loaded in a catalytic site by prior incubation of the subcomplexes with ADP and Mg^{2+}. The failure of these mutant subcomplexes to dissociate inhibitory MgADP from a catalytic site when ATP binds to noncatalytic sites is reflected in their maximal velocities and their responses to increasing concentrations of Mg^{2+} in the assay medium. The maximal velocities of the $(\alpha R304C)_3\beta_3\gamma$ and $(\alpha Y300C)_3\beta_3\gamma$ subcomplexes are similar to that of the $(\alpha D269N)_3\beta_3\gamma$ subcomplex which is 6.0 μmol of ATP hydrolyzed mg^{-1} min^{-1} (33% of that of wild type) (*7*). The fact that the mutant $(\alpha R304C)_3\beta_3\gamma$, $(\alpha Y300C)_3\beta_3\gamma$, and $(\alpha D269N)_3\beta_3\gamma$ subcomplexes retain considerable ATPase activity reflects that MgADP binds to a single catalytic site of MF_1 or TF_1 in active (F_1·MgADP) and inactive (F_1*·MgADP) conformations which slowly interconvert (*31*, *32*). The mutant $(\alpha R304C)_3\beta_3\gamma$ and $(\alpha Y300C)_3\beta_3\gamma$ subcomplexes are progressively inhibited to a greater extent than wild-type as the Mg^{2+} concentration in the assay medium increased, indicating a higher propensity to entrap inhibitory MgADP in a catalytic site of these mutants during turnover.

The $(\alpha Y300C)_3\beta_3\gamma$ subcomplex appears to have severely diminished cooperativity. Its ATPase activity is slightly accelerated by LDAO compared to that of the wild-type and $(\alpha R304C)_3\beta_3\gamma$ subcomplexes. More importantly, the rate of formation of the inhibitory ADP−fluoroaluminate complex increases only 40% when two catalytic sites are loaded with MgADP as opposed to one. The rate of formation of the inhibitory ADP−fluoroaluminate complex promoted by P_i or SO_3^{2-} in the presence of excess ADP was also greatly attenuated compared to those of the wild-type and other mutant subcomplexes. The observation that ADP−fluoroaluminate complexes appear to be formed in three catalytic sites of the $(\alpha Y300C)_3\beta_3\gamma$ subcomplex, as opposed to two with the other subcomplexes, is consistent with the argument that negative cooperativity of binding nucleotides in catalytic sites is diminished in this mutant subcomplex.

In contrast, the $(\alpha F244C)_3\beta_3\gamma$ subcomplex appears to have enhanced cooperativity between noncatalytic and catalytic sites. Unlike the wild-type and other mutant subcomplexes, the ATPase activity of the $(\alpha F244C)_3\beta_3\gamma$ subcomplex is not sensitive to increasing concentrations of Mg^{2+} in the assay medium, indicating a greatly decreased propensity to entrap inhibitory MgADP in a catalytic site during turnover. Furthermore, it forms ADP−fluoroaluminate complexes in two catalytic sites at rates considerably greater than that of wild type in the presence of excess ADP under various conditions. This behavior reflects the fact that the ADP−fluoroaluminate complexes are formed from the active F_1·MgADP complex rather than from the inactive F_1*·MgADP complex, which was previously demonstrated with other mutant subcomplexes (*22*). The $(\alpha F244C)_3\beta_3\gamma$ subcomplex has the unusual property of retaining MgADP in a noncatalytic site after gel permeation chromatography when ADP−fluoroaluminate complexes are bound to two catalytic sites. In the crystal structure of MF_1 (*4*), the phenolic oxygen of αTyr244 is 19.4 Å from the γ-phosphate and 26.7 Å from the C^8 of AMP−PNP bound to noncatalytic sites. The fact that αF244 is distant from bound nucleotides, yet substituting it with Cys both increases affinity of noncatalytic sites for ADP and affects the rate of formation of ADP−fluoroaluminate complexes in catalytic sites, suggests that this residue participates in propagation of conformational signals

between noncatalytic and catalytic sites. Although αR304 and αY300 are conserved in all F_1-ATPases that have been sequenced, either Tyr or Phe is present at position α244. Therefore, it might be argued that the side chain of αF244 of TF_1 does not interact with the side chain of αR304. However, it has been shown that cation−π interactions exist in proteins (*33*). Therefore, in TF_1 the side chain of αF244 might interact with the side chain of αR304 by a cation−π interaction mimicking the hydrogen bonding of αY244 with αR304 in MF_1.

The functional role of noncatalytic nucleotide binding sites in F_1-ATPases is unclear. Although chemical modification of these sites or disruption of these sites by mutagenesis partly or completely abolishes ATP hydrolysis (*7*, *34*−*37*), the initial rate of hydrolysis of ATP is the same whether these sites are saturated with ATP (*10*). However, when noncatalytic sites are not saturated with ATP, inhibitory MgADP accumulates in a catalytic site during turnover (*7*, *10*, *11*). Furthermore, Richard et al. (*38*) have shown that light-induced ATP synthesis by TF_oF_1 co-reconstituted into liposomes with bacteriorhodopsin is stimulated by liganding noncatalytic sites with ATP. The behavior of these mutants raises the possibility that liganded noncatalytic nucleotide binding sites have primarily a structural role in maintaining the integrity of the pathway for transmitting conformational signals from one catalytic site to another during catalysis.

ACKNOWLEDGMENT

We thank Matthew Stelzer for his help in preparing the $(\alpha Y300C)_3\beta_3\gamma$ mutant subcomplex.

REFERENCES

1. Pedersen, P. L., and Amzel, L. M. (1993) *J. Biol. Chem. 268*, 9937−9940.
2. Allison, W. S., Jault, J.-M., Zhuo, S., and Paik, S. R. (1992) *J. Bioenerg. Biomembr. 24*, 469−477.
3. Cross, R. L. (1992) in *Molecular Mechanisms in Bioenergetics* (Ernster, L., Ed.) pp 317−330, Elsevier Science Publishers, Amsterdam.
4. Abrahams, J. P., Leslie, A. G., Lutter, R., and Walker, J. E. (1994) *Nature 370*, 621−628.
5. Yokoyama, K., Hisabori, T., and Yoshida, M. (1989) *J. Biol. Chem. 264*, 21837−21841.
6. Paik, S. R., Yokoyama, K., Yoshida, M., Ohta, T., Kagawa, Y., and Allison, W. S. (1993) *J. Bioenerg. Biomembr. 25*, 679−684.
7. Jault, J.-M., Matsui, T., Jault, F. M., Kaibora, C., Muneyuki, E., Yoshida, M., Kagawa, Y., and Allison, W. S. (1995) *Biochemistry 34*, 16412−16418.
8. Jault, J.-M., Dou, C., Grodsky, N. B., Matsui, T., Yoshida, M., and Allison, W. S. (1996) *J. Biol. Chem. 271*, 28818−28824.
9. Matsui, T., and Yoshida, M. (1995) *Biochim. Biophys. Acta 1231*, 139−146.
10. Jault, J.-M., and Allison, W. S. (1993) *J. Biol. Chem. 268*, 1558−1566.
11. Paik, S. R., Jault, J.-M., and Allison, W. S. (1994) *Biochemistry 33*, 126−133.
12. Vasilyeva, E. A., Minkov, I. B., Fitin, A. F., and Vinogradov, A. D. (1982) *Biochem. J. 202*, 9−14.
13. Drobinskaya, I. Y., Koslov, I. A., Murataliev, M. B., and Vulfson, F. N. (1985) *FEBS Lett. 182*, 419−424.
14. Verburg, J. G., and Allison, W. S. (1990) *J. Biol. Chem. 265*, 8065−8074.
15. Omote, H., Park, M.-Y., Maeda, M., and Futai, M. (1994) *J. Biol. Chem. 269*, 10265−10269.
16. Hartog, A. F., Edel, C. M., Braham, J., Muijsers, A. O., and Berden, J. A. (1997) *Biochim. Biophys. Acta 1318*, 107−122.
17. Jault, J.-M., and Allison, W. S. (1994) *J. Biol. Chem. 269*, 319−325.
18. Penefsky, H. S. (1977) *J. Biol. Chem. 252*, 2891−2899.
19. Kunkel, T. A., Benebek, K., and McClary, T. (1991) *Methods Enzymol. 204*, 125−129.
20. Prober, J. M., Trainor, G. L., Dam, R. J., Hobbs, F. W., Robertson, C. W., Zagursky, R. J., Cocuzza, A. J., Jensen, M. A., and Baumeister, K. (1987) *Science 238*, 336−341.
21. Bradford, M. M. (1976) *Anal. Biochem. 72*, 248−254.
22. Dou, C., Grodsky, N. B., Matsui, T., Yoshida, M., and Allison, W. S. (1997) *Biochemistry 36*, 3719−3727.
23. Guerrero, K. J., Xue, Z., and Boyer, P. D. (1990) *J. Biol. Chem. 265*, 16280−16287.
24. Murateliev, M. B. (1992) *Biochemistry 31*, 12885−12892.
25. Yoshida, M., and Allison, W. S. (1986) *J. Biol. Chem. 261*, 5714−5721.
26. Jault, J.-M., and Allison, W. S. (1994) *FEBS Lett. 347*, 13−16.
27. Kironde, F. A. S., Parsonage, D., and Senior, A. E. (1989) *Biochem. J. 259*, 421−426.
28. Wilke-Mounts, S., Pagan, J., and Senior, A. E. (1995) *Arch. Biochem. Biophys. 324*, 153−158.
29. Walker, J. E., Saraste, M., Runswick, M. J., and Gay, N. J. (1982) *EMBO J. 1*, 945−951.
30. Otsuka, A., Yoshida, M., and Allison, W. S. (1981) *J. Biol. Chem. 256*, 9084−9089.
31. Milgrom, Y. M., and Murateliev, M. B. (1989) *Biochim. Biophys. Acta 975*, 50−58.
32. Bulygin, V. V., and Vinogradov, A. D. (1991) *Biochem. J. 276*, 149−156.
33. Dougherty, D. A. (1996) *Science 271*, 163−168.
34. Bullough, D. A., and Allison, W. S. (1986) *J. Biol. Chem. 261*, 5722−5730.
35. Weber, J., Bowman, C., Wilke-Mounts, S., and Senior, A. E. (1995) *J. Biol. Chem. 270*, 21045−21049.
36. Yohda, M., Ohta, S., Hisabori, T., and Kagawa, Y. (1988) *Biochim. Biophys. Acta 933*, 156−164.
37. Matsui, T., Muneyuki, E., Honda, M., Allison, W. S., Dou, C., and Yoshida, M. (1997*) J. Biol. Chem. 272*, 8215−8221.
38. Richard, P., Pitard, B., and Rigaud, J.-L. (1995) *J. Biol. Chem. 270*, 21571−21578.
39. Guggenheim, E. A. (1926) *Philos. Mag. 2*, 538−543.

BI972349D